RSC Advances

PAPER

View Article Online
View Journal | View Issue

Cite this: *RSC Adv.*, 2025, **15**, 732

Terpene polymerization *via* a binary neodymium-based catalytic system with di-*n*-butylmagnesium as a co-catalyst†

Teresa Córdova,[a] Francisco Javier Enriquez-Medrano,[a] Ilse Magaña,[a] Maricela García-Zamora,[a] Nelson A. Jimenéz-Reyes,[a] José M. Mata-Padilla,[a] Edgar E. Cabrera-Álvarez,[b] Luis Valencia *[c] and Ramón Díaz de León*[a]

Received 18th October 2024
Accepted 18th December 2024

DOI: 10.1039/d4ra07481e

rsc.li/rsc-advances

The development of materials from renewable resources has been increasing, intending to reduce the consumption of fossil sources, with terpenes being one of the main families that reduce the consumption of isoprene. The study of the binary catalytic system neodymium versatate/dibutyl magnesium (NdV_3/Mg(*n*-Bu)$_2$), for the coordination homopolymerization of β-myrcene and β-farnesene, was carried out analysing different [Nd] : [Mg] ratios (between 4 and 10). Reporting conversions of 92% and 83% at an [Nd] : [Mg] ratio of 8 for polymyrcene (PMy) and polyfarnesene (PFa), respectively, and microstructures comprising 1,4 content above 80% for both polymers (PMy, *cis*-59% and PFa, *cis*-83%). It was observed that PFa samples presented a higher 1,4-*cis* content in relation to PMy samples, presumably due to the size of the side group present in the monomer structure and due to steric hindrance; similarly, a 3,4 content of 14% (PMy) and 10% (PFa) was observed. The glass transition temperature of the PMy samples ranged from −63.7 °C to −66.5 °C, while for the PFa samples, it was between −75.4 °C and −75.5 °C. The binary [Nd] : [Mg] system used in the study predominantly exhibited a 1,4-*cis* content at [Nd] : [Mg] ratios of 8.

Introduction

The advancement of sustainable and eco-friendly materials has emerged as a cornerstone in polymer science, motivated by increasing global concerns over environmental degradation and the depletion of fossil fuel reserves.[1–3] This paradigm shift reflects a fundamental change in material science, emphasizing the development of innovative approaches to address sustainability challenges. Among these, the utilization of renewable resources as alternatives to petroleum-based raw materials has gained significant attention. Recent progress in polymerization techniques, such as visible-light-induced radical polymerization and light-controlled reversible addition–fragmentation chain transfer (RAFT) polymerization, has further expanded the potential for creating advanced materials. These methods, facilitated by quantum dot (QD) photocatalysts like cadmium selenide (CdSe), enable precise control over polymer architecture and open avenues for designing hybrid organic–inorganic nanocomposites.[4,5] Such advancements not only contribute to reducing the environmental footprint but also demonstrate the versatility and functionality of next-generation polymeric materials, aligning with the broader goals of sustainability and innovation in material science.

As a class of biobased monomers, terpenes have received considerable attention in this context.[6–8] Their intrinsic renewable nature and wide prevalence in plant resins and essential oils make them an attractive alternative to some traditional petroleum-based monomers for polymer synthesis, like butadiene.[9–12] In our previous study, we successfully synthesized high molecular weight polyterpenes *via* coordinative chain transfer polymerization using a ternary Ziegler–Natta catalyst system, resulting in a predominantly *cis* microstructure.[13] This research, just like multiple others in the literature,[10,14–20] has readily demonstrated the potential of terpenes as viable monomers for creating sustainable polymers.

Recent studies have further elucidated the role of monomer structure in determining polymer microstructure, particularly in systems utilizing magnesium-based co-catalysts.[21] Notably, in the polymerization of isoprene and butadiene, the use of a binary system with [Mg(*n*-Bu)$_2$] can lead to polymers with high *trans* isomer contents.[22] It is crucial to elucidate the influence of this co-catalyst on the microstructural characteristics during the polymerization of renewable terpenes, such as β-myrcene

[a]*Research Center for Applied Chemistry, Blvd Enrique Reyna 140, Saltillo 25294, Mexico. E-mail: Ramon.diazdeleon@ciqa.edu.mx*

[b]*CONAHCYT, Research Center for Applied Chemistry, Unidad Monterrey, Av. Alianza Sur 204, Apodaca, Nuevo León, C.P. 66629, Mexico*

[c]*Biofiber Tech Sweden AB, Norrsken House, Birger Jarlsgatan 57 C, Stockholm, Sweden. E-mail: Luisalex_val@hotmail.com*

† Electronic supplementary information (ESI) available: NMR spectra and gel permeation chromatographs. See DOI: https://doi.org/10.1039/d4ra07481e

and β-farnesene, particularly considering the impact of the larger side chains of these monomers.

The current study has two main objectives: first, to evaluate the effects of introducing [Mg(*n*-Bu)$_2$] as a co-catalyst on critical parameters, including molecular weight, microstructure, and polymer yield, which refers to the consumption of monomer during the reaction; and second, to increase the understanding of how modified catalytic systems can be employed to produce tailored polymers from renewable resources for specific applications. We anticipate that the insights obtained from this research will contribute significantly to the advancement of sustainable polymer synthesis approaches.

Results and discussion

Polymerization behaviour and physical properties of polymers

The polymerization of β-myrcene using the neodymium-based catalytic system, in conjunction with di-*n*-butylmagnesium ([Mg(*n*-Bu)$_2$]) as a co-catalyst was systematically explored in this research work, elucidating the effects of various reaction parameters on the polymerization behaviour and the properties of the resulting polymers. A conceptual schematic illustration of the monomers, catalysts, and co-catalysts used in this scientific work is shown in Fig. 1.

The yield of the polyterpenes showed significant variations depending on the ratios used in the catalytic system. Specifically, the [Nd] : [Mg] ratio, representing the molar proportion between neodymium and magnesium, and the [Mon] : [Nd] ratio, corresponding to the molar proportion between the monomer and neodymium, had a notable impact on the results obtained, as detailed in Table 1, where yield refers to the monomer consumption during the reaction, which is determined through gravimetric analysis. A higher [Nd] : [Mg] ratio generally led to higher yields, indicating that the presence of [Mg(*n*-Bu)$_2$] is favourable for the polymerization process. For instance, Run My2 with a 1 : 6 ratio of [Nd] : [Mg] achieved an 85.4% yield, which is notably higher than the 38% yield of Run My1 with a 1 : 4 ratio. This variation can be attributed to the role of [Mg(*n*-Bu)$_2$] in the catalytic system, which can engage in multiple functions: it can act as Lewis's acid to increase the electrophilicity of the neodymium catalyst, facilitate monomer insertion into the growing chain and also serve as chain transfer agent (CTA) to modulate molecular weight. Overall, it appears that a higher amount of [Mg(*n*-Bu)$_2$] leads to higher yields, as it better activates the neodymium catalyst at higher ratios – by influencing the steric environment around the catalytic centre, facilitating monomer insertion by affecting the spatial arrangement around the active site.

Conversely, in Run My4, we observed a lower yield compared to Run My3 despite a higher [Nd] : [Mg] ratio. This could be indicative of a more complex interplay of factors that affect the polymerization process. Several potential reasons could account for this deviation from the expected trend. For instance, at higher [Mg(*n*-Bu)$_2$] concentrations, there may be competitive coordination to the neodymium centre, which could sterically hinder the approach of monomer molecules, thus reducing the polymerization rate and overall yield. It is possible that an excessive amount of co-catalyst forms stable complexes that are less active in the polymerization process or even impact the solubility and miscibility of the catalyst system complexes, which can adversely affect the yield. Additional experimentation would be necessary to elucidate this behaviour more thoroughly.

The molecular weights (M_n and M_w) exhibited considerable variability, suggesting that, indeed, the [Mg(*n*-Bu)$_2$] co-catalyst is influencing the initiation and propagation steps of the polymerization. Initially, as the [Mg(*n*-Bu)$_2$] concentration increases, it may enhance the activation of the neodymium catalyst, leading to more efficient monomer insertion and longer polymer chains, thus increasing M_n and M_w, as can be seen with Run My2 compared to My1. However, as the concentration of [Mg(*n*-Bu)$_2$] continues to increase, the chain transfer activity may become predominant, effectively shortening the growing polymer chains and reducing the molecular weight, as observed for My4. This is because the chain transfer reaction competes with chain propagation, leading to the termination of the growing chains and the formation of new ones. The balance between propagation and termination rates is crucial. This would also explain the increase in polydispersity index (PDI) as the molecular weight distribution becomes broader with more frequent chain transfers reactions.

Fig. 2 shows more clearly the correlation between the [Mg] : [Nd] ratio and the yield, M_w, and PDI of the polymyrcene

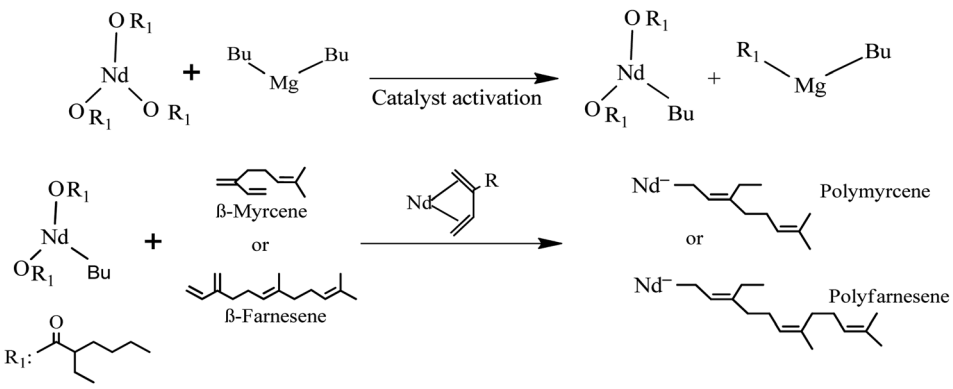

Fig. 1 Conceptual schematic illustration of the synthesis of terpenes in this work.

Table 1 β-Myrcene polymerization parameters and physical properties of polymerized terpenes

Run[a]	[Nd] : [Mg][b]	[Mon] : [Nd]	Time (h)	T (°C)	Yield (%)	M_n[c] (kg mol^{-1})	M_w[c] (kg mol^{-1})	PDI[c]	N_p
My1	1 : 4	250	140	50	38.0	32.0	112.1	3.5	0.40
My2	1 : 6	250	140	50	85.4	77.4	546.6	7.0	0.38
My3	1 : 8	250	140	50	92.0	62.9	550.0	8.7	0.50
My4	1 : 10	250	140	50	85.2	51.9	283.6	5.4	0.56
My5	1 : 6	250	114	60	50.3	44.9	289.6	6.4	0.38
My6	1 : 8	250	114	60	90.4	107.9	647.6	5.9	0.29
My7	1 : 10	250	114	60	88.2	82.3	528.0	6.4	0.36
My8	1 : 8	250	43	70	66.4	64.2	279.5	4.3	0.35
My9	1 : 10	250	48	70	84.2	92.8	560.2	6.0	0.31
My10	1 : 8	500	67	70	92.5	77.9	464.2	5.9	0.40
My11	1 : 10	500	67	70	86.3	47.7	335.4	7.0	0.62

[a] Experimental conditions: cyclohexane = 50.9 mL and monomer = 10 mL. [b] [NdV_3] : [Mg(n-Bu)$_2$] molar ratio. [c] Determined by size exclusion chromatography using polystyrene standards. [Nd] = 2.29 × 10^{-4} mol, [Mon] = 5.73 × 10^{-2} mol, N_p: average number of polymer chains produced by a single Nd atom.

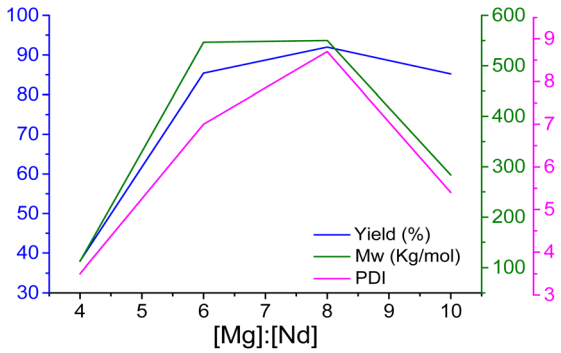

Fig. 2 Influence of [Nd] : [Mg] ratio on polymyrcene properties at 50 °C (My1–My4).

reactions, showing the behaviour and elucidating the catalytic system's capacity to modulate polymer characteristics and underpinning the design considerations for tailored material synthesis.

The average number of polymer chains produced by a single Nd atom (N_p) was calculated by dividing the total number of polymer chains formed by the total number of Nd atoms used in the reaction. This calculation helps to understand the efficiency of the catalytic system in terms of chain initiation and propagation.

Notably, at the optimal [Mg] : [Nd] ratio of 8, observed in Fig. 2, the average number of polymer chains produced per Nd atom (N_p) also reaches its maximum. This suggests that the catalytic efficiency in terms of chain initiation and propagation is highest at this ratio. The enhanced N_p at a ratio of 8 can be attributed to the co-catalyst [Mg(n-Bu)$_2$] significantly improving the activation of the neodymium catalyst, thereby increasing the number of active sites available for polymer chain initiation. This results in more polymer chains being formed per Nd atom. Furthermore, the optimal ratio ensures a favorable spatial arrangement around the catalytic centre, facilitating efficient monomer insertion and reducing steric hindrance.

The polymerization of β-farnesene, as documented in Table 2, was also conducted under various conditions to investigate the influence of the [Nd] : [Mg], and [Mon] : [Nd] ratios, time, and temperature on the yield, molecular weight, and PDI. Like the earlier findings with β-myrcene, the data from β-farnesene polymerization also presents an intricate interplay of these factors. The yield of β-farnesene polymers exhibited notable variations with changes in the [Nd] : [Mg] and [Mon] : [Nd] ratios. For instance, Fa2 with a 1 : 8 [Nd] : [Mg] ratio showed a significantly higher yield (83.9%) compared to Fa1 (19%) with a 1 : 6 ratio. This suggests that, as observed with β-myrcene, the presence of [Mg(n-Bu)$_2$] positively impacts the polymerization

Table 2 β-Farnesene polymerization parameters and physical properties of polymerized terpenes

Run[a]	[Nd] : [Mg][b]	[Mon] : [Nd]	Time (h)	T (°C)	Yield (%)	M_n[c] (kg mol^{-1})	M_w[c] (kg mol^{-1})	PDI[c]	N_p
Fa1	1 : 6	150	92	70	19.0	47.0	137.0	2.8	0.12
Fa2	1 : 8	150	92	70	83.9	178.3	852.7	4.7	0.14
Fa3	1 : 6	150	92	60	37.2	34.8	91.5	2.6	0.33
Fa4	1 : 8	150	92	60	55.6	172.0	982.5	5.7	0.10
Fa5	1 : 10	150	92	60	35.3	106.0	625.3	5.8	0.10
Fa6	1 : 10	250	92	60	20.0	16.0	213.5	13.3	0.38

[a] Experimental conditions: cyclohexane = 50.9 mL and monomer = 10 mL. [b] [NdV_3] : [Mg(n-Bu)$_2$] molar ratio. [c] Determined by size exclusion chromatography using polystyrene standards. [Nd] = 2.91 × 10^{-4} mol, [Mon] = 4.37 × 10^{-2} mol. N_p: average number of polymer chains produced by a single Nd atom (N_p).

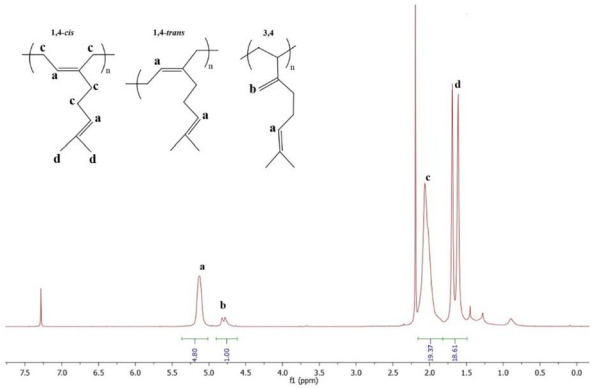

Fig. 3 ^{1}H NMR spectra, corresponding to Run My2, in order to illustrate the signal assignment in a polymyrcene sample.

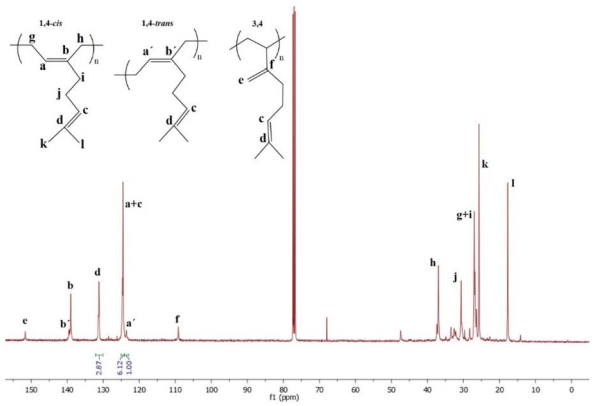

Fig. 4 ^{13}C NMR spectra, corresponding to Run My2, in order to illustrate the signal assignment in a polymyrcene sample.

process, potentially enhancing catalyst activation and monomer insertion efficiency.

The M_n and M_w displayed considerable variability across different runs. This aligns with the trends observed in β-myrcene polymerization, where increasing [Mg(*n*-Bu)$_2$] concentrations initially lead to higher molecular weights. However, a further increase can result in reduced molecular weight due to enhanced chain transfer activity. For example, Fa3 shows a dramatic decrease in Mn compared to Fa2, likely due to this chain transfer effect. The PDI values in β-farnesene polymerization varied significantly, indicating the influence of [Mg(*n*-Bu)$_2$] in chain transfer activities.

The M_n and M_w displayed considerable variability across different runs. This aligns with the trends observed in β-myrcene polymerization, where increasing [Mg(*n*-Bu)$_2$] concentrations initially lead to higher molecular weights. However, a further increase can result in reduced molecular weight due to enhanced chain transfer activity. For example, Fa3 shows a dramatic decrease in M_n compared to Fa2, likely due to this chain transfer effect. The PDI values in β-farnesene polymerization varied significantly, indicating the influence of [Mg(*n*-Bu)$_2$] in chain transfer activities. Higher PDIs, as seen in Fa6 (13.3), suggest a broader distribution of molecular weights, which can be attributed to the increased chain transfer activity at higher [Mg(*n*-Bu)$_2$] concentrations.

The resulting polymyrcene and polyfarnesene samples' microstructure was analyzed using ^{1}H and ^{13}C NMR spectroscopy. The NMR data allowed for the assignment of key structural motifs, particularly the *cis*-1,4, *trans*-1,4, and 3,4 additions, which are crucial for determining the polymer's stereoregularity. Fig. 3 presents the ^{1}H NMR spectrum of Run My2, highlighting the characteristic proton signals corresponding to the various isomers. Similarly, Fig. 4 shows the ^{13}C NMR spectrum of Run My2, illustrating the carbon signals and facilitating the identification of stereoisomers in the polymer chain.

The microstructure of resulting polymyrcene and polyfarnesene samples, as analyzed by ^{1}H and ^{13}C NMR, predominantly exhibits *cis*-configurations, a finding that starkly contrasts with the high *trans*-content observed in the polymerization of 1,3-butadiene. This contrast is particularly highlighted in the work of Zheng *et al.*,[22] where their system produced polybutadienes with around 96% *trans*-1,4 content, moderate molecular weights, and narrow polydispersity. The significant difference in stereoregularity between the terpene polymers and polybutadiene underscores the influential role of monomer side chains in determining polymer microstructure.

Table 3 Microstructure and thermal properties of polymerized terpenes

Run[a]	[Nd] : [Mg][b]	T (°C)	3,4[c] (%)	1,4[c] (%)	1,4-*cis*[d] (%)	1,4-*trans*[d] (%)	T_g[e] (°C)
My1	1 : 4	50	17.4	82.6	55.8	26.8	−65.5
My2	1 : 6	50	15.1	84.9	57.9	27	−65.6
My3	1 : 8	50	14.5	85.5	59.9	25.6	−65.7
My6	1 : 8	60	20	80	62.0	18.0	−66.1
My8	1 : 8	70	18	82	53.8	28.2	−63.1
My10	1 : 8	70	14.7	85.3	59.8	25.3	−63.7
Fa1	1 : 6	70	10.5	89.5	83.8	5.7	−75.4
Fa2	1 : 8	70	9.5	90.5	78.5	12.0	−75.4
Fa4	1 : 8	60	8.6	91.4	74.8	16.6	−75.5
Fa5	1 : 10	60	8.6	91.4	72.5	18.9	−75.5

[a] Experimental conditions: cyclohexane = 50.9 mL and monomer = 10 mL. [b] [NdV$_3$]/[Mg(*n*-Bu)$_2$] molar ratio. [c] Regioselectivity determined by ^{1}H NMR. [d] Stereoselectivity determined by ^{13}C NMR. [e] Glass transition temperature determined by DSC at 5 °C min^{-1}.

The presence of larger side chains in β-myrcene and β-farnesene likely contributes to a sterically hindered environment that promotes *cis* configurations during polymerization. This steric effect appears to override the influence of [Mg(*n*-Bu)$_2$], which, in the case of butadiene, promotes the formation of *trans*-14-polymers.

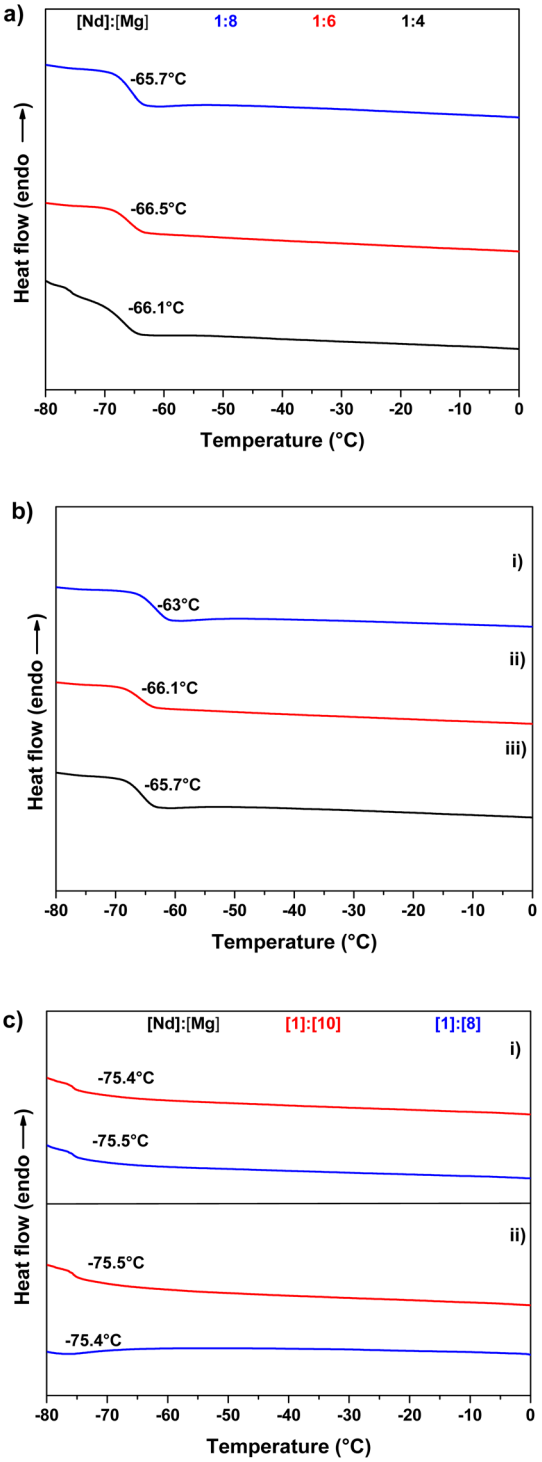

Fig. 5 Thermograms of polymerized terpenes: (a) β-myrcene polymerized at 50 °C with varying [Nd] : [Mg] ratios. (b) β-Myrcene polymerized at varying temperatures: (i) 70 °C, (ii) 60 °C and (iii) 50 °C. (c) β-Farnesene polymerized at (i) 60 °C and (ii) 70 °C with varying [Nd] : [Mg] ratios.

The Table 3 for example, examining specific β-myrcene runs reveals this trend: My1, with a 1 : 4 [Nd] : [Mg] ratio at 50 °C, displays a 53.3% *cis* content. My2, with a 1 : 6 [Nd] : [Mg] ratio at the same temperature, shows an increased *cis* content of 59.9%. My3, with a 1 : 8 [Nd] : [Mg] ratio, continues this pattern, also exhibiting a *cis* content of 59.9%. Furthermore, My6, with a 1 : 8 [Nd] : [Mg] ratio but at a higher temperature of 60 °C, demonstrates a further increase in *cis* content to 62%. These percentages for 1,4 *cis* and 1,4 *trans* correspond to the proportion of the 1,4 microstructure obtained from proton NMR. These results indicate that a higher co-catalyst content slightly increases the *cis* content in β-myrcene polymers, emphasizing the significant impact of monomer structure on polymer microstructure.

In β-farnesene polymers, this trend is consistently observed. Runs like Fa2 and Fa3, both conducted at a temperature of 70 °C but with different [Nd] : [Mg] ratios of 1 : 8 and 1 : 10, respectively, show high *cis* contents of 83.8% and 78.5%. This consistency in both β-myrcene and β-farnesene polymers suggests a generalizable effect of monomer structure on the microstructure of the resulting polymers, highlighting the pivotal role of monomer side chains in the stereoregularity of polymers produced with [Mg(*n*-Bu)$_2$] as part of the catalytic system.

The differential scanning calorimetry (DSC) analysis of the polymyrcene and polyfarnesene samples revealed glass transition temperatures (T_g) below −60 °C. In Fig. 5a, the effect of increasing the [Nd] : [Mg] ratio is observed, showing that this increase does not significantly impact the T_g of polymyrcene, which remains within a narrow range between −65 °C and −66.1 °C. On the other hand, for polyfarnesene (Fig. 5c), an increase in the [Nd] : [Mg] ratio results in a significant decrease in T_g, with values between −75.4 °C and −75.5 °C, suggesting that polyfarnesene exhibits greater flexibility at low temperatures compared to polymyrcene. As shown in Fig. 5b, in polymyrcene samples, increasing the reaction temperature from 50 °C to 70 °C leads to a slight decrease in T_g, particularly in the My8 and My10 samples, which show values of −63.1 °C and −63.7 °C, respectively. This behavior suggests that the flexibility of the materials is directly related to their chemical and topological structure. In the present study, it was observed that polyfarnesene exhibits lower glass transition temperatures compared to polymyrcene, which can be attributed to its higher content of saturated groups and a more branched structure, promoting greater molecular mobility.

Experimental

Materials

All experimental manipulations were executed within an MBraun glove box under an inert argon atmosphere or *via* standard Schlenk line techniques. β-Myrcene (My, sourced from Aldrich) and β-farnesene (Fa, supplied by AMYRIS) were purified through distillation over sodium under an argon environment. Neodymium versatate (NdV_3, procured from Strem Chemicals) and the co-catalyst dibutyl magnesium (Mg(*n*-Bu)$_2$,

obtained from Aldrich) were utilized as received. Cyclohexane, acquired from Aldrich, underwent distillation from sodium under an argon atmosphere to ensure purity.

Catalyst activation and polymerization

In an MBraun glove box or under an inert nitrogen atmosphere, all catalyst manipulations were carried out in oven-dried bottles that were nitrogen-purged and sealed with a rubber septum for subsequent magnetic stirring. The catalyst components, namely [NdV_3] and [Mg(*n*-Bu)$_2$], were sequentially added to the reaction vessel. The catalyst mixture was then allowed to age at room temperature for 30 minutes prior to the polymerization reaction.

Polymerizations were carried out in 30 mL glass vials, each equipped with a magnetic stir bar and secured to ensure a consistent nitrogen atmosphere. The reaction vial was charged with the monomer and cyclohexane, and the mixture was heated to the desired temperature while being stirred at 150 rpm. Upon reaching the target temperature, the pre-aged catalyst system was introduced into the reactor. Samples were taken at intervals to monitor the progress of the polymerization and to determine the polymer yield through gravimetric analysis. The reaction was quenched with acidified methanol, and the polymers were stabilized using Irganox 1076. The resulting materials were precipitated in methanol and dried under vacuum at 25 °C to constant weight.

Characterization techniques

The molecular weights of the samples were determined through size exclusion chromatography (SEC) employing a PLGel mixed column in a Hewlett-Packard instrument (HPLC series 1100) equipped with a refractive index detector. Calibration was performed with polystyrene standards, and tetrahydrofuran (HPLC grade from Aldrich) served as the eluent at a flow rate of 1 mL min^{-1}.

Differential scanning calorimetry (DSC) thermograms were acquired using a TA Instrument DSC 2000. The analyses were performed under an inert atmosphere with a heating rate of 5 °C min^{-1}, and each sample was analyzed twice to eliminate thermal history effects.

Microstructure analyses of polymyrcene and polyfarnesene samples were conducted using ^{1}H and ^{13}C nuclear magnetic resonance (NMR) on a Bruker Ultrashield Plus 400 MHz spectrometer. $CDCl_3$ was utilized as a solvent, and the analyses were carried out at room temperature. The isomer 3,4 in relation to the isomer 1,4 (*cis* + *trans*) was determined by the ^{1}H NMR spectrum, integrating signals in the olefinic group region from 4.7 to 5.3 ppm. The *cis*/*trans* ratio was calculated by the ^{13}C NMR spectrum (proton-gated decoupling no-NOE experiments), integrating signals of olefinic groups. The Fig. 6 show the microstructure schematics.

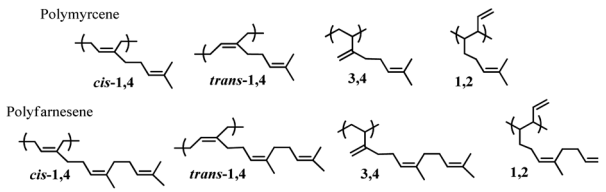

Fig. 6 Microstructure schematics.

Conclusions

In conclusion, this study shows the intricate relationship between catalytic systems and monomer structure in the polymerization of terpenes. We have shown that the use of [Mg(*n*-Bu)$_2$] as a co-catalyst in conjunction with a neodymium-based catalyst can significantly influence the yield, molecular weight, and microstructure of polyterpenes. Our research suggests that monomer side chains are crucial in defining the polymer microstructure, with the substantial side chains of β-myrcene and β-farnesene favouring a dominance of *cis* configurations. This effect is significant enough to even override the stereoselective tendencies of [Mg(*n*-Bu)$_2$], observed in other systems like the polymerization of butadiene reported by W. Zheng *et al.*[22] The T_g has reinforced our understanding of the polymers' thermal properties, revealing the impact of monomer side chains and the [Nd] : [Mg] ratio on the polymers' flexibility and stability.

Furthermore, our findings underscore the versatility of [Mg(*n*-Bu)$_2$] in producing polymers with varied microstructures, an aspect significantly influenced by the inherent characteristics of the monomers. This accentuates the importance of monomer design in predicting polymer properties, which is crucial for the development of new catalytic systems aimed at sustainable polymer synthesis. The microstructural analysis of β-myrcene and β-farnesene polymers exemplifies the decisive role of monomer side chains in influencing stereoregularity, a factor that prevails over the catalytic system's inherent selectivity.

This study represents a contribution to the quest for sustainable material alternatives. By elucidating the effects of catalyst systems on terpene-based polymer synthesis, we pave the way for future advancements in renewable polymers tailored for specific applications.

Data availability

The data used and analyzed during the development of this work is available in the ESI files accompanying this document.†

Conflicts of interest

There are no conflicts to declare.

Acknowledgements

To Consejo Nacional de Humanidades, Ciencia y Tecnologías (CONAHCYT) for the financial support provided for the completion of Córdova's postdoctoral fellowship. The authors gratefully acknowledge the financial support of CONAHCYT CF-2023-I-2151 "Estudio para controlar las propiedades mecánicas,

antiflama y degradabilidad en el ambiente de nuevos biocompuestos poliméricos sustentables", and (CONAHCyT) Mexico (grant no. 320630) "Descubrimiento y diseño de nuevos materiales termoeléctricos híbridos orgánicos/inorgánicos con alta eficiencia termoeléctrica". And the financial support of the Research Center for Applied Chemistry (CIQA) through the internal project 6752.

References

1 A. Gandini and T. M. Lacerda, *Molecules*, 2022, **27**(1), 159.
2 A. Kindler and O. Zelder, in *Synthetic Biodegradable and Biobased Polymers: Industrial Aspects and Technical Products*, ed, A. Künkel, G. Battagliarin, M. Winnacker, B. Rieger and G. Coates, Springer International Publishing, Cham, 2024, pp. 1–33.
3 I. Magaña, R. López, F. J. Enríquez-Medrano, S. Kumar, A. Aguilar-Sanchez, R. Handa, R. de León and L. Valencia, *J. Mater. Chem. A*, 2022, **10**, 5019–5043.
4 Y. Zhu and E. Egap, *Polym. Chem.*, 2020, **11**, 1018–1024.
5 Y. Zhu, E. Ramadani and E. Egap, *Polym. Chem.*, 2021, **12**, 5106–5116.
6 F. Della Monica and A. W. Kleij, *Polym. Chem.*, 2020, **11**, 5109–5127.
7 M. E. G. Mosquera, G. Jiménez, V. Tabernero, J. Vinueza-Vaca, C. García-Estrada, K. Kosalková, A. Sola-Landa, B. Monje, C. Acosta, R. Alonso and M. Á. Valera, *Sustainable Chem.*, 2021, **2**, 467–492.
8 C. Wahlen and H. Frey, *Macromolecules*, 2021, **54**, 7323–7336.
9 P. Sarkar and A. K. Bhowmick, *RSC Adv.*, 2014, **4**, 61343–61354.
10 R. E. de León Gómez, F. J. Enríquez-Medrano, H. Maldonado Textle, R. Mendoza Carrizales, K. Reyes Acosta, H. R. López González, J. L. Olivares Romero and L. E. Lugo Uribe, *Can. J. Chem. Eng.*, 2016, **94**, 823–832.
11 L. Valencia, F. J. Enríquez-Medrano, H. R. López González, R. Handa, H. S. Caballero, R. M. Carrizales, J. L. Olivares-Romero and R. E. de León Gómez, *RSC Adv.*, 2020, **10**, 36539–36545.
12 R. Díaz de León, R. López, L. Valencia, R. Mendoza, J. Cabello and J. Enríquez, *Key Eng. Mater.*, 2018, **779**, 115–121.
13 T. Córdova, F. J. Enríquez-Medrano, E. M. Cartagena, A. B. Villanueva, L. Valencia, E. N. C. Álvarez, R. L. González and R. Díaz-de-León, *Polymers*, 2022, **14**(14), 2907.
14 P. Sahu and J. S. Oh, *Ind. Eng. Chem. Res.*, 2022, **61**, 11815–11824.
15 M. C. C. de Sá, T. Córdova, P. A. Melo, R. D. de León and J. C. Pinto, *Can. J. Chem. Eng.*, 2023, **101**, 5256–5269.
16 A. Banda-Villanueva, J. L. González-Zapata, M. E. Martínez-Cartagena, I. Magaña, T. Córdova, R. López, L. Valencia, S. G. Medina, A. M. Rodríguez, F. Soriano and R. de León, *Polymers*, 2022, **14**(7), 1406.
17 J. Liu, X. Fan, X. Min, X. Zhu, N. Zhao and Z. Wang, *RSC Adv.*, 2018, **8**, 21926–21932.
18 P. Sarkar and A. K. Bhowmick, *ACS Sustainable Chem. Eng.*, 2016, **4**, 5462–5474.
19 J. Hilschmann and G. Kali, *Eur. Polym. J.*, 2015, **73**, 363–373.
20 J. Zhang, C. Aydogan, G. Patias, T. Smith, L. Al-Shok, H. Liu, A. M. Eissa and D. M. Haddleton, *ACS Sustainable Chem. Eng.*, 2022, **10**, 9654–9664.
21 A. Ventura, T. Chenal, M. Bria, F. Bonnet, P. Zinck, Y. Ngono-Ravache, E. Balanzat and M. Visseaux, *Eur. Polym. J.*, 2013, **49**, 4130–4140.
22 W. Zheng, N. Yan, Y. Zhu, W. Zhao, C. Zhang, H. Zhang, C. Bai, Y. Hu and X. Zhang, *Polym. Chem.*, 2015, **6**, 6088–6095.